11th International Symposium on Turbulence and Shear Flow Phenomena (TSFP11)
Southampton, UK, July 30 to August 2, 2019

STRUCTURES AND CHARACTERISTICS OF TURBULENT HEAT TRANSFER IN COMBINED-CONVECTION TURBULENT BOUNDARY LAYER ON INCLINED FLAT PLATE

H. Hattori
Information and Analysis Technologies Division
Nagoya Institute of Technology
Gokiso-cho, Showa-ku, Nagoya 466-8555, Japan
hattori@nitech.ac.jp

K. Oura, H. Okabe, T. Houra and M. Tagawa
Department of Electrical and Mechanical Engineering
Nagoya Institute of Technology

ABSTRACT

The objective of this study is to reveal structures and characteristics of turbulent heat transfer in combined-convection turbulent boundary layer on an inclined flat plate by means of DNS. DNS reproduces the spatially-developing both velocity and thermal turbulent boundary layers on an inclined flat plate, but a thermal boundary layer does not simultaneously develop with a velocity boundary layer due to the entrance region of thermal field which is caused by the wall thermal condition. In comparison with cases of horizontal or vertical flat plate whose buoyant effect only works in a direction, it is found that different tendencies of characteristic turbulent statistics and structures are clearly obtained in the case of an inclined flat plate. This is because the effect of buoyancy obviously works both the streamwise and the wall-normal velocities in the combined-convection boundary layer on an inclined flat plate. Thus, the DNS reveals structures and characteristics of turbulent heat transfer in combined-convection turbulent boundary layer on an inclined flat plate.

INTRODUCTION

Since a combined-convection turbulent boundary layer whose characters has both a natural and a forced convections is often encountered in various heat transfer fields, it is important issue to reveal structures and characteristics of heat transfer in that convection. In a combined-convection turbulent boundary layer, it can be considered that a different heat transfer phenomena can be observed due to the direction of buoyant force, i.e., the case of heat transfer on the horizontal plate is different from the case on the vertical plate. The structures of turbulent heat transfer in a combined-convection turbulent boundary layer on a horizontal flat plate where the direction of streamwise velocity crosses the direction of buoyant force at right angles has been revealed by means of direct numerical simulation (DNS) (Hattori *et al.*, 2007, 2014). Also, it is also revealed that the different characters of turbulent heat transfer phenomenon in the combined-convection turbulent boundary layer on a vertical flat plate (Hattori *et al.*, 2017) can be observed in comparison with the boundary layer on a horizontal flat plate, because the direction of wall-normal velocity crosses the direction of buoyant force at right angles in this case, i.e., the buoyancy directly works the streamwise velocity field. On the other hand, in a combined-convection turbulent boundary layer on inclined flat plate, since the buoyancy influences both a streamwise and a wall-normal velocities, it can be considered that more complicated structures and characteristics of turbulent heat transfer phenomenon are observed. Incidentally, concerning the thermal field, a thermal boundary layer develops on the heating wall which is heated from a midstream of flow field, i.e., an entrance region of thermal field which gives a higher heat transfer rate is often observed in various actual thermal fields. Thus, to know the characteristics of turbulent heat transfer in an entrance region is an important issue. The combined-convection turbulent boundary layer with an entrance region of thermal field on a horizontal or a vertical flat plate has been investigated using DNS in detail, in which the remarkable variations of turbulent statistics and structures influenced by temperature difference between wall and free stream are revealed. (Hattori *et al.*, 2017, 2015). There is not, however, much a knowledge of turbulent heat transfer phenomena of combined-convection turbulent boundary layer with an entrance region of thermal field on an inclined flat plate. Thus, objectives of this study are to conduct the DNS of combined-convection turbulent boundary layer with an entrance region of thermal field on an inclined flat plate, and to reveal structures and characteristics of heat transfer in such the turbulent boundary layer.

PROCEDURE OF DNS

Assuming that the Boussinesq approximation is approved for the Navier-Stokes equation, the governing equations used in the present DNS are indicated as follows (Hattori *et al.*, 2007):

$$\frac{\partial u_i}{\partial t} + u_j \frac{\partial u_i}{\partial x_j} = -\frac{1}{\rho}\frac{\partial p}{\partial x_i} + \nu \frac{\partial^2 u_i}{\partial x_j \partial x_j} - \delta_{ik} g_k \beta \Delta\Theta \quad (1)$$

$$\frac{\partial u_i}{\partial x_i} = 0 \quad (2)$$

$$\frac{\partial \theta}{\partial t} + u_j \frac{\partial \theta}{\partial x_j} = \alpha \frac{\partial^2 \theta}{\partial x_j \partial x_j} \quad (3)$$

where the Einstein summation convention applies to repeated indices. The buoyancy term in Eq. (1) becomes

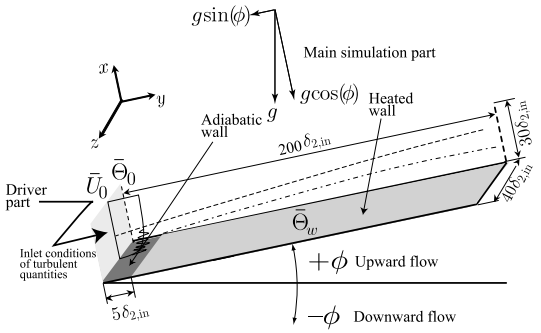

Figure 1. Computational domain, coordinate system and wall thermal conditions

$g_1 = g\sin(\phi)$ for $k = 1$, $g_2 = g\cos(\phi)$ for $k = 2$ and $g_3 = 0$ for $k = 3$.

The configuration of computational domain which is composed by driver and main simulation parts, coordinate system and wall thermal conditions are shown in Fig. 1, where the wall of main simulation part is heated by an isothermal condition from $x/\delta_{2,\mathrm{in}} = 5$ to the downstream direction in order to form the entrance region of thermal field. The present DNS is carried out using the methods of high accuracy finite difference method (Hattori *et al.*, 2007) and of generation of turbulent inflow data for both the velocity and the thermal fields (Hattori *et al.*, 2007; Lund *et al.*, 1998; Kong *et al.*, 2000). The grid points and domain size are arranged by $x \times y \times z = 192 \times 128 \times 128 = 100\delta_{2,\mathrm{in}} \times 30\delta_{2,\mathrm{in}} \times 40\delta_{2,\mathrm{in}}$ and $384 \times 128 \times 128 = 200\delta_{2,\mathrm{in}} \times 30\delta_{2,\mathrm{in}} \times 40\delta_{2,\mathrm{in}}$ for the driver and main simulation parts, respectively. Here, $\delta_{2,\mathrm{in}}$ is the momentum thickness at the inlet of driver part. As for the grid resolution normalized by the local inner scale, which is the fundamental parameter of DNS, the relevance of grid resolution in our DNS has been confirmed in several DNS of turbulent boundary layer (Hattori *et al.*, 2007, 2014). Thus, it is evident that the grid resolutions of this DNS properly satisfy DNS requirements as compared with the previous DNS (Hattori *et al.*, 2007, 2014). The Reynolds number, $Re_{\delta_{2,\mathrm{in}}}$, is 300 and the Prandtl number, Pr, is 0.71. In the case of wall temperature which is higher than the free stream temperature, $\bar{\Theta}_w > \bar{\Theta}_0$, the Richardson number is -0.005. This condition causes the unstable thermal stratification in the case of horizontal plate. On the other hand, the Richardson number is 0.005 in the case of wall temperature which is lower than the free stream temperature, $\bar{\Theta}_w < \bar{\Theta}_0$ (This condition causes the stable thermal stratification in the case of horizontal plate), and $Ri_{\delta_{2,\mathrm{in}}} = 0$ is for the neutral condition. Also, inclined angles of flat plate are set to $\phi = 0,\ \pm\pi/8,\ \pm\pi/4,\ \pm 3\pi/8$ and $\pm\pi/2$, where the flat plate becomes a horizontal flat plate when the case of $\phi = 0$, and a vertical flat plate when $\phi = \pi$. The cases of negative sign of inclined angle indicate a downward flow, i.e., the buoyancy influences to a similar with direction of streamwise velocity. The boundary conditions are similar with the previous study of turbulent boundary layer (Hattori *et al.*, 2007).

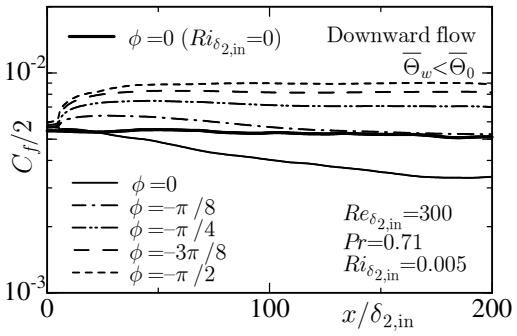

(a) Downward flow

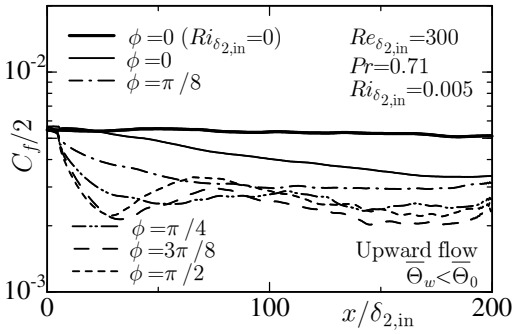

(b) Upward flow

Figure 2. Profiles of local wall friction coefficients along inclined flat plate ($\bar{\Theta}_w < \bar{\Theta}_0$)

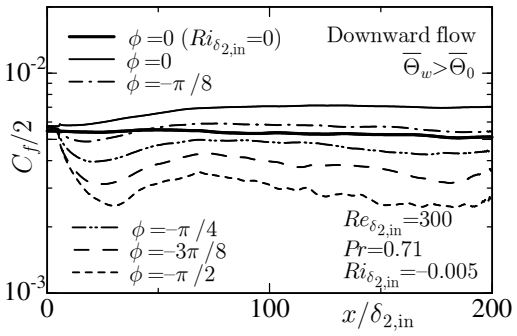

(a) Downward flow

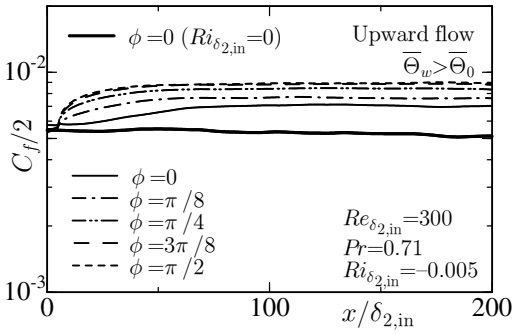

(b) Upward flow

Figure 3. Profiles of local wall friction coefficients along inclined flat plate ($\bar{\Theta}_w > \bar{\Theta}_0$)

RESULTS AND DISCUSSION

Figures 2 and 3 show profiles of local wall friction coefficients along the inclined flat plate in all cases. In Fig. 2, the results of horizontal plate with the neutral and stable thermal stratifications are included for comparison, where the condition of difference of temperature between wall and free stream is $\bar{\Theta}_w < \bar{\Theta}_0$. In the case of downward flow, the local wall friction coefficients, $C_f/2$, increase with decreasing angle of flat plate ($\phi = -\pi/8 \sim -\pi/2$), but $C_f/2$ decrease with increasing the angle of flat plate

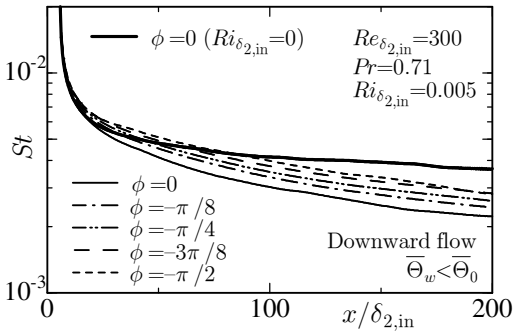

(a) Downward flow

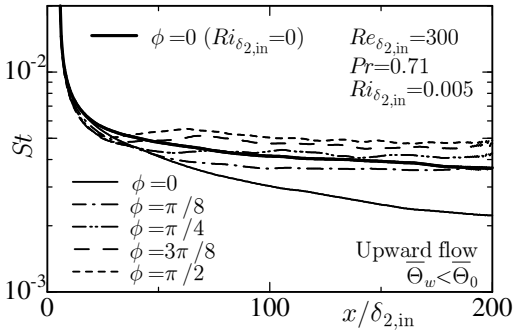

(b) Upward flow

Figure 4. Profiles of local Stanton numbers along inclined flat plate ($\bar{\Theta}_w < \bar{\Theta}_0$)

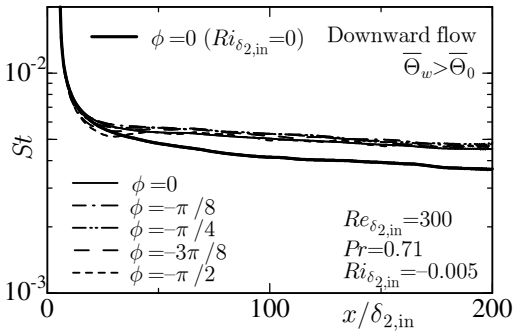

(a) Downward flow

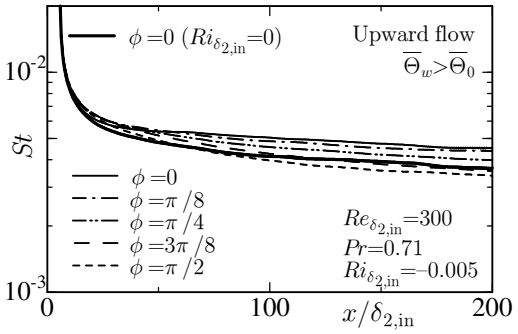

(b) Upward flow

Figure 5. Profiles of local Stanton numbers along inclined flat plate ($\bar{\Theta}_w > \bar{\Theta}_0$)

($\phi = \pi/8 \sim \pi/2$) in the case of upward flow. In the case of $\phi = \pm\pi/8, \pm\pi/4$ and $\pm 3\pi/8$, the buoyancy influences both the streamwise and wall-normal velocities, but the buoyancy affects the different direction of the streamwise velocity for the cases of downward and upward flow, i.e., the

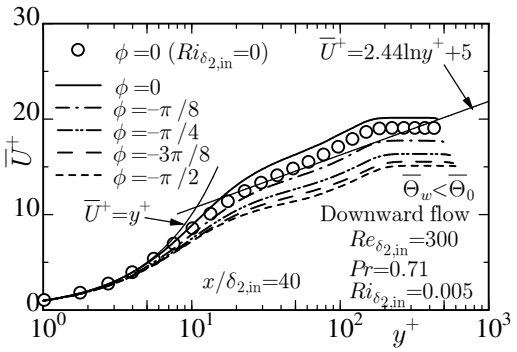

(a) Downward flow

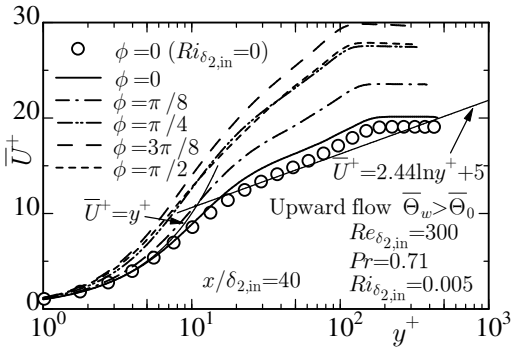

(b) Upward flow

Figure 6. Distributions of mean velocities along inclined flat plate ($\bar{\Theta}_w < \bar{\Theta}_0$)

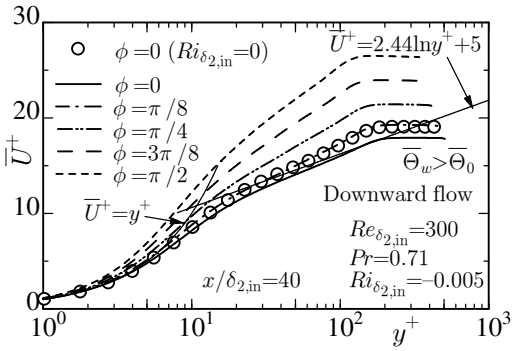

(a) Downward flow

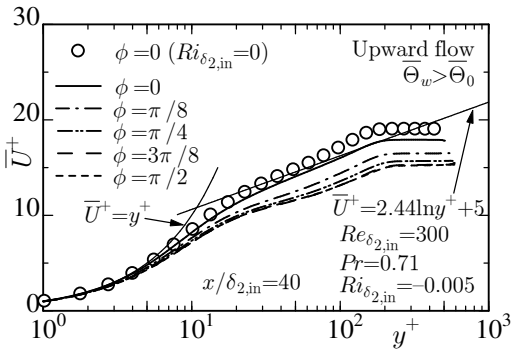

(b) Upward flow

Figure 7. Distributions of mean velocities along inclined flat plate ($\bar{\Theta}_w > \bar{\Theta}_0$)

buoyancy works in the same direction of streamwise velocity in the case of downward flow. Therefore, it is found

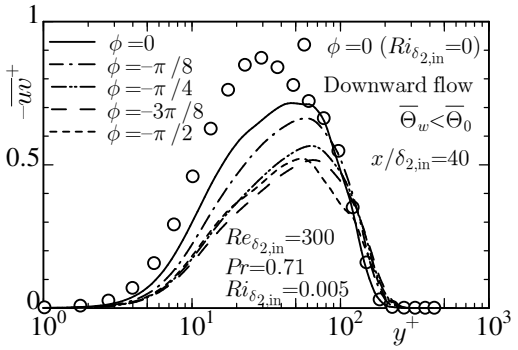

(a) Downward flow

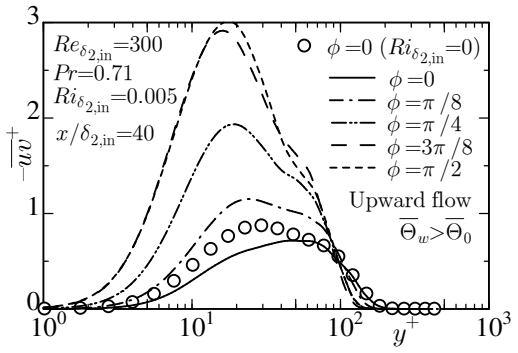

(b) Upward flow

Figure 8. Distributions of Reynolds shear stresses along inclined flat plate ($\bar{\Theta}_w < \bar{\Theta}_0$)

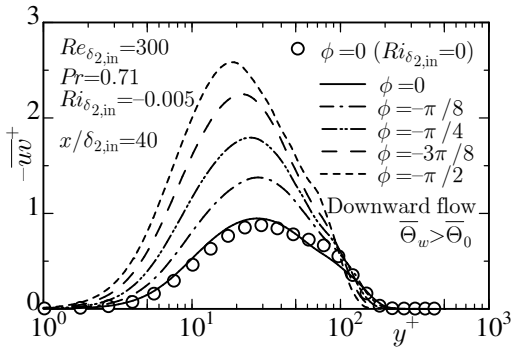

(a) Downward flow

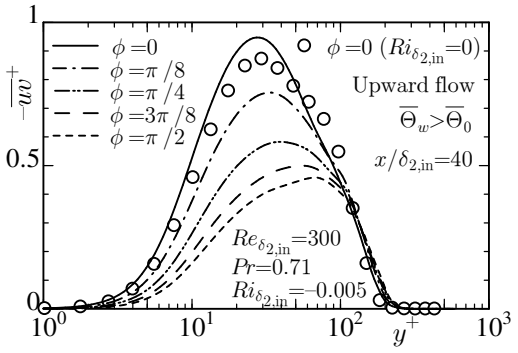

(b) Upward flow

Figure 9. Distributions of Reynolds shear stresses along inclined flat plate ($\bar{\Theta}_w > \bar{\Theta}_0$)

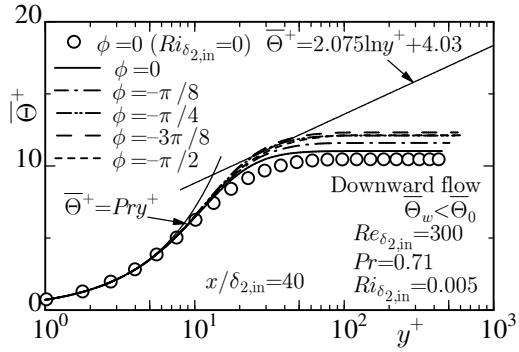

(a) Downward flow

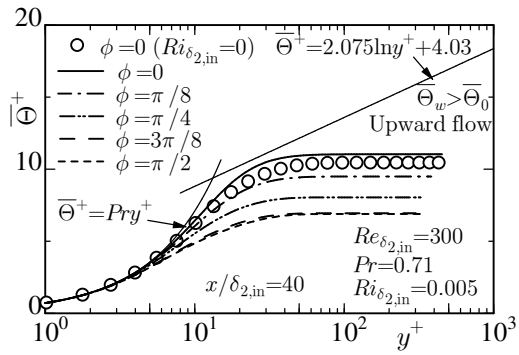

(b) Upward flow

Figure 10. Distributions of mean temperature along inclined flat plate ($\bar{\Theta}_w < \bar{\Theta}_0$)

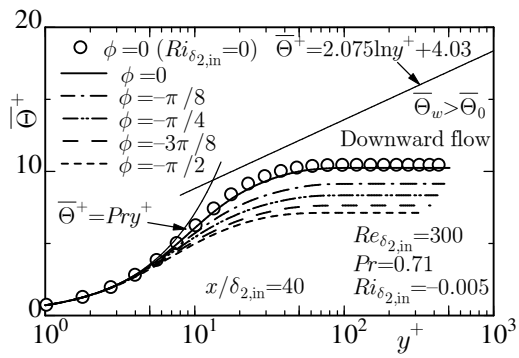

(a) Downward flow

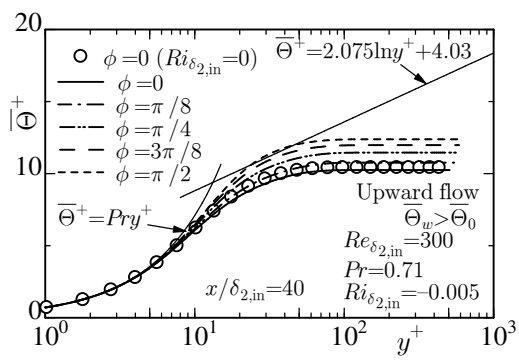

(b) Upward flow

Figure 11. Distributions of mean temperature along inclined flat plate ($\bar{\Theta}_w > \bar{\Theta}_0$)

that increase and decrease of $C_f/2$ is varied by the direction of buoyancy in the streamwise direction. As for the condition of difference of temperature between wall and free stream is $\bar{\Theta}_w > \bar{\Theta}_0$ as shown in Fig. 3, local friction coef-

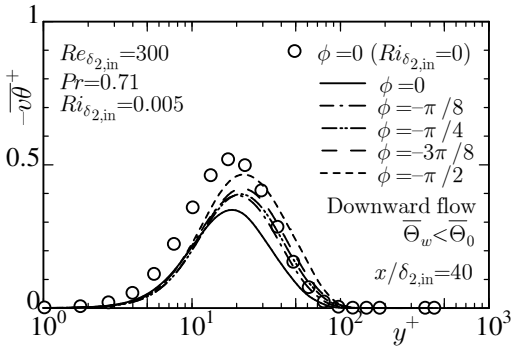

(a) Downward flow

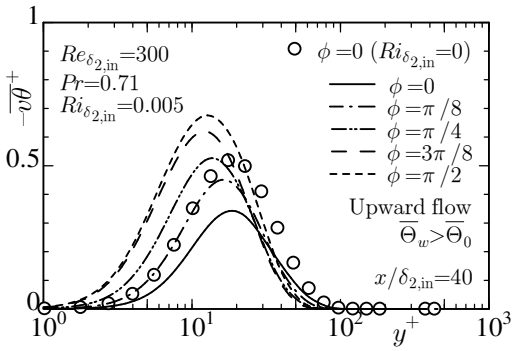

(b) Upward flow

Figure 12. Distributions of wall-normal turbulent heat fluxes along inclined flat plate ($\bar{\Theta}_w < \bar{\Theta}_0$)

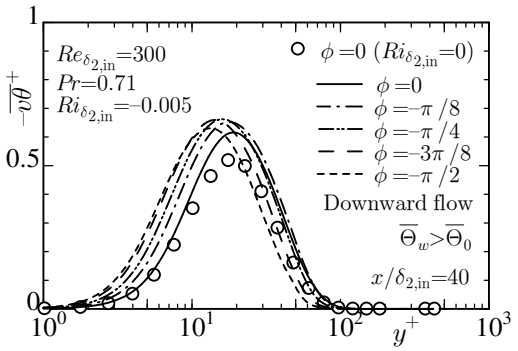

(a) Downward flow

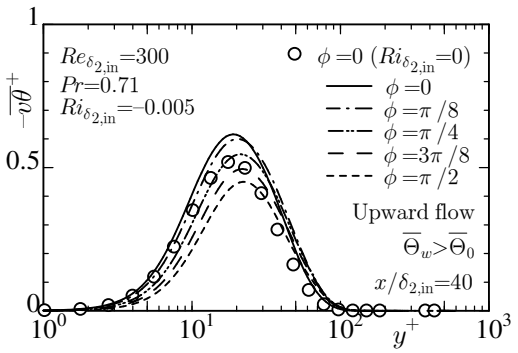

(b) Upward flow

Figure 13. Distributions of wall-normal turbulent heat fluxes along inclined flat plate ($\bar{\Theta}_w > \bar{\Theta}_0$)

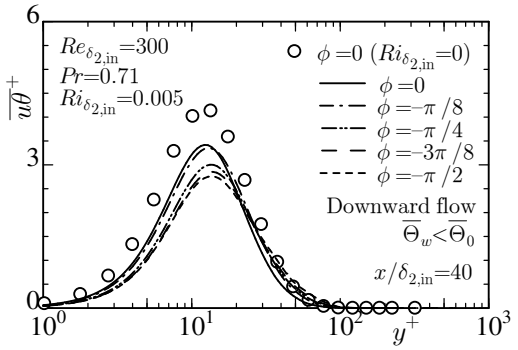

(a) Downward flow

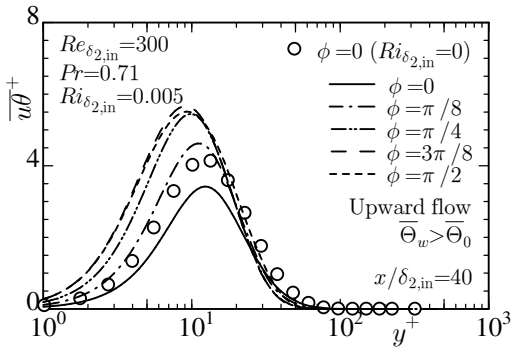

(b) Upward flow

Figure 14. Distributions of streamwise turbulent heat fluxes along inclined flat plate ($\bar{\Theta}_w < \bar{\Theta}_0$)

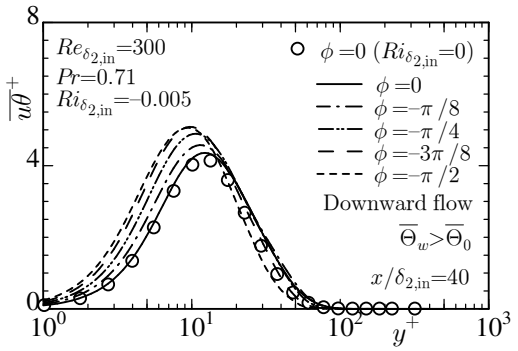

(a) Downward flow

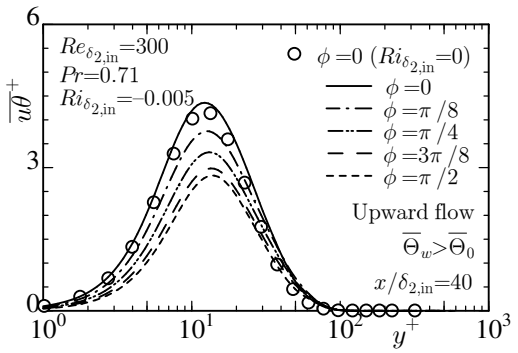

(b) Upward flow

Figure 15. Distributions of streamwise turbulent heat fluxes along inclined flat plate ($\bar{\Theta}_w > \bar{\Theta}_0$)

ficients decrease toward the downstream region in the case of downward flow. However, in the case of $-\pi/4$, C_f is greater than that of the case of neutral thermal stratification in the downstream region. Thus, it is considered that the ef-

fect of unstable thermal stratification remains in this region. In the case of upward flow, the local wall friction coefficients of inclined flat plate increase similar with the case of horizontal flat plate with the unstable thermal stratification. Also, increase and decrease of $C_f/2$ is varied by the direction of buoyancy in the streamwise direction in the case of $\bar{\Theta}_w > \bar{\Theta}_0$.

The profiles of local Stanton numbers along inclined flat plate are shown in Figs. 4 and 5. In the case of $\bar{\Theta}_w < \bar{\Theta}_0$, the local Stanton numbers, *St*, are smaller than that of the case of neutral thermal stratification, but *St* increases with decreasing angle of flat plate ($\phi = -\pi/8 \sim -\pi/2$) in the downward flow. In the upward flow, *St* increases with increasing angle of flat plate ($\phi = \pi/8 \sim \pi/2$), where the local Stanton numbers of the cases of large angle of flat plate whose angles exceed $\pi/4$ are larger than that of case of neutral thermal stratification in the downstream region. Therefore, it can be seen that the effect of buoyancy in the streamwise direction works for the local Stanton number increase with increasing angle of flat plate, but the local Stanton numbers in the downward flow do not exceed that of the case of neutral thermal stratification even if the angle is $\pi/2$ (vertical flat plate). On the other hand, in the case of $\bar{\Theta}_w > \bar{\Theta}_0$ as shown in Fig. 5, the local Stanton numbers are almost larger than that of the case of neutral thermal stratification. In the downward flow, the local Stanton numbers are almost same in cases of all angle. On the other hand, the local Stanton number decrease with increasing angle of flat plate in the upward flow, in which the local Stanton number is smaller than that of the case of neutral thermal stratification in the case of vertical flat plate ($\phi = \pi/2$).

In order to observe turbulent statistics which affect the local wall friction coefficient, Figures 6∼9 show distributions of streamwise mean velocity and Reynolds shear stresses. In the case of $\bar{\Theta}_w < \bar{\Theta}_0$, the profiles of mean velocity drop in the log-law region without the case of $\phi = 0$ in the downward flow. In the upward flow, it can be seen that the profiles of mean velocity greatly stay out of the universal log-law profile from the small viscus sublayer as indicated in Fig. 6(b). On the other hand, in the case of $\bar{\Theta}_w > \bar{\Theta}_0$, the largest profile of mean velocity is given in the case of vertical flat plate in the downward flow. It can be seen that, however, the profiles are almost similar in the upward flow as shown in Fig. 7(b). As for the distributions of Reynolds shear stress, the appearance large Reynolds shear stresses are observed in the case of $\bar{\Theta}_w < \bar{\Theta}_0$ in the upward flow as shown in Fig. 8(b) due to great decrease of local wall friction coefficient, where the profiles of mean velocity stay out of the universal log-law toward upper side. This tendency can be also observed in the case of $\bar{\Theta}_w > \bar{\Theta}_0$ in the downward flow as shown in Fig. 9(a).

As for the thermal field, distributions of mean temperature, wall-normal turbulent heat flux and streamwise turbulent heat flux are shown in Figs. 10∼15. Due to entrance region of thermal filed, the mean temperature does not fully developed in the calculation region, i.e., the clear log-law profiles of mean temperature is not found at $x/\delta_{2,\mathrm{in}} = 40$ as indicated in Figs. 10 and 11. In cases of $\bar{\Theta}_w < \bar{\Theta}_0$ in the downward flow and $\bar{\Theta}_w > \bar{\Theta}_0$ in the upward flow, it can be seen that the mean temperature of vertical flat plate ($\phi = \pi/2$) develops faster than other cases. On the other hand, in the cases of $\bar{\Theta}_w < \bar{\Theta}_0$ in the upward flow and $\bar{\Theta}_w > \bar{\Theta}_0$ in the downward flow, it can be observed that wall-normal turbulent heat fluxes distribute at the conductive sublayer more in comparison with other cases. as shown in Figs. 12 and 13. Thus, these distributions influence the profiles of mean temperature as indicated in Figs. 10(b) and 11(a). Finally, the streamwise turbulent heat flux which remarkably affects the distributions of turbulent quantities in the combined-convection turbulent boundary layer is shown in Figs. 14 and 15. Also, the distributions of streamwise turbulent heat fluxes in the conductive sublayer can be found in the cases of $\bar{\Theta}_w < \bar{\Theta}_0$ in the upward flow and $\bar{\Theta}_w > \bar{\Theta}_0$ in the downward flow. These distributions of both the turbulent heat fluxes clearly affect the distributions of Reynolds shear stresses as indicated in Figs. 8(b), because the turbulent heat fluxes are contained in the buoyancy term in the transport equation on the inclined flat plate.

CONCLUSIONS

Structures and characteristics of turbulent heat transfer in a combined-convection turbulent boundary layer on an inclined flat plate are revealed by means of DNS. On the inclined flat plate, cases of different temperature difference between wall and free stream with the positive angle of flat plate (upward flow) or the negative angle of flat plate (downward flow) are investigated. In comparison with cases of horizontal or vertical flat plates whose buoyant effect only works in a direction, it is found that different tendencies of characteristic turbulent statistics and structures are clearly obtained.

ACKNOWLEDGEMENTS

This work was supported by JSPS KAKENHI Grant Number 17K06195 and grant of collaborative research of AICE.

REFERENCES

Hattori, H., Hotta, K. & Houra, T. 2014 Characteristics and structures in thermally-stratified turbulent boundary layer with counter diffusion gradient phenomenon. *International Journal of Heat and Fluid Flow* **49**, 53 – 61.

Hattori, H., Hotta, K., Houra, T. & Tagawa, M. 2015 Dns of thermal entrance region in thermally-stratified turbulent boundary layer. *Proceedings of the Asian Symposium on Computational Heat Transfer and Fluid Flow -ASCHT2015* .

Hattori, H., Houra, T. & Nagano, Y. 2007 Direct numerical simulation of stable and unstable turbulent thermal boundary layers. *International Journal of Heat and Fluid Flow* **28**, 1262–1271.

Hattori, H., Oura, K., Houra, T. & Tagawa, M. 2017 Dns of combined-convection turbulent boundary layer on vertical heated flat plate. *Proceedings of 16th European Turbulence Conference -ETC16* .

Kong, H, Choi, H & Lee, J S 2000 Direct Numerical Simulation of Turbulent Thermal Boundary Layers. *Physics of Fluids* **12**, 2555–2568.

Lund, T. S., Wu, X. & Squires, K. D. 1998 Generation of turbulent inflow data for spatially-developing boundary layer simulation. *Journal of Computational Physics* **140**, 233–258.